67

Strain Localization in Geomaterials

*PIs: Hiroko Kitajima[1, *], Amine Benzerga[2], Janet Bluemel[3]*
Students: Vigneshwaran Radhakrishnan[2], Patrick Hubbard[3], Milan Brankovic[1], and Daniel Brandenburg[1]
1. Department of Geology & Geophysics, 2. Department of Aerospace Engineering, 3. Department of Chemistry (Corresponding Author Email: kitaji@tamu.edu)

T3: TEXAS A&M TRIADS FOR TRANSFORMATION
A President's Excellence Fund Initiative

Introduction

Strain localization plays an important role in the performance and behavior of many materials that are crucial for our lives. It is observed in the deformation of various materials including soils, concrete, rocks, metals, and polymers. In engineered materials, the onset of strain localization implies failure. In geomaterials, strain localization affects subsequent motions and plate tectonics with potential consequences on earthquake dynamics. Strain localization spans a wide range of length scales from a nanometer scale in metallic glass to kilometers of shear zones in the Earth's crust.

This project integrates mechanical modeling, laboratory experiments, and chemical characterization to investigate deformation and localization processes in geomaterials. We have conducted basic deformation experiments at elevated pressures and characterize the evolution of mechanical and chemical properties occurring during these deformation and localization processes. The characterization will span from the molecular level to macroscopic mapping on a scale of millimeters. In parallel, we have developed a mechanical model to study and document the localization in the materials. The following sections describe our most important research results in more detail.

Micromechanics Framework

A variational definition of the effective yield surface, $\partial\mathscr{C}$:

$$\Sigma_{ij} = \frac{\partial \Pi}{\partial D_{ij}}(\mathbf{D}), \qquad \Pi(\mathbf{D}) = (1-f)\inf_{\mathbf{v}\in\mathcal{K}(\mathbf{D})} \langle \sup_{\sigma^*\in\mathcal{C}} \sigma^*_{ij} d_{ij} \rangle_{\Omega\setminus\omega} \quad (1)$$

Basic elements of any model are therefore:

1. the geometry of the elementary cell;
2. a micro-scale plasticity model, i.e., the boundary of $\mathcal{C}$ and a flow rule; and
3. kinematically admissible (trial) velocity fields, $\mathbf{v}$, defining the set $\mathcal{K}(\mathbf{D})$.

Homogeneous yielding: $\forall \mathbf{X} \in \partial\Omega, \quad \mathbf{x} = \mathbf{F}\mathbf{X}$ or equivalently, $\mathbf{v} = \mathbf{D}\mathbf{x}$ where $\mathbf{F}$ and $\mathbf{D}$ are constants.

Flow potential of the form $\Phi(\mathbf{\Sigma}; f, w, \mathbf{n}^{(3)}, \bar{\sigma})$ (Keralavarma and Benzerga, 2010):

$$\Phi(\mathbf{\Sigma}) = C\frac{3}{2}\frac{\mathbf{\Sigma} : \mathbb{H} : \mathbf{\Sigma}}{\bar{\sigma}^2} + 2(g+1)(g+f)\cosh\left(\kappa\frac{\mathbf{\Sigma} : \mathbf{X}}{\bar{\sigma}}\right) - (g+1)^2 - (g+f)^2$$

$$\mathbb{H} = \mathbb{J} : \mathbb{h} : \mathbb{J} + \eta(\mathbf{X}\otimes\mathbf{Q} + \mathbf{Q}\otimes\mathbf{X})$$

$$\mathbf{X} = \alpha_2(\mathbf{n}^{(1)}\otimes\mathbf{n}^{(1)} + \mathbf{n}^{(2)}\otimes\mathbf{n}^{(2)}) + (1-2\alpha_2)\mathbf{n}^{(3)}\otimes\mathbf{n}^{(3)}$$

$$\mathbf{Q} = -\frac{1}{2}(\mathbf{n}^{(1)}\otimes\mathbf{n}^{(1)} + \mathbf{n}^{(2)}\otimes\mathbf{n}^{(2)}) + \mathbf{n}^{(3)}\otimes\mathbf{n}^{(3)}$$

Criterion parameters (κ, g, α_2...) may depend on f, w and 3 independent scalar invariants of Hill's tensor $\mathbb{h}$.

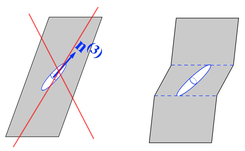

In shear, inhomogeneous yielding prevails from the outset (Drucker, 1966).
This result holds irrespective of void shape.

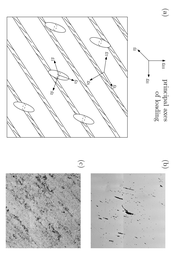

Rice's Localization Criterion (1976)

$$\det(\mathbf{M}) = 0$$

$$M_{jl} = n_i K^{tan}_{ijkl} n_k$$

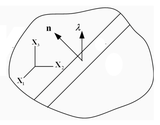

Fig. 1. Schematic representation of the localization band.

- Localization is impossible for an *isotropic* von-Mises like *hardening* material.
- Axisymmetric states are extremely stiff against shear band formation.

Simulations on Instability in Compression

Basic fact:
Shear fracture in cylindrical pins of several anisotropic materials

Hypothesis:
Plastic anisotropy drives shear fracture.

Kondori, PhD thesis 2015

h_{TS}/h_L=5.0 Θ=30°; n=0.01

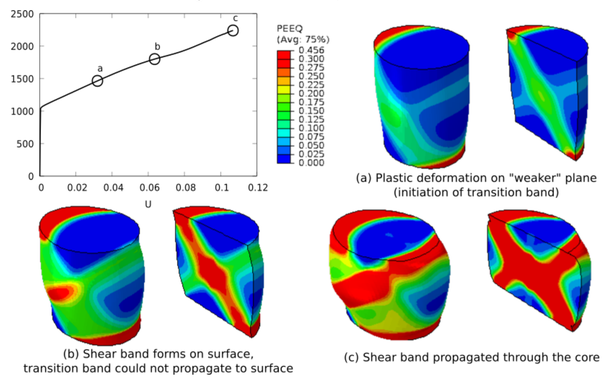

(a) Plastic deformation on "weaker" plane (initiation of transition band)

(b) Shear band forms on surface, transition band could not propagate to surface

(c) Shear band propagated through the core

Compaction of Controlled Pore Glass (CPG)

Controlled pore glass (CPG) particles, which are composed of silicon dioxide grains with networks of nanopores, are compacted under elevated pressure while P-wave velocity (v_p) is measured. All the three CPG samples with different grain size and nano-pore size indicate and increase in vp with pressure. v_p decreases with nano-pore diameter. Water-saturated CPG shows higher v_p than dry samples.

CPG Mesh Size	Grain Size (μm)	Nanopore Diameter (nm)	Nanopore Porosity (%)	Initial Macropore Porosity
35-65	250-500	60	62	0.68
100-200	74-149	30	47	0.51
200-425	34-74	150	72	0.70

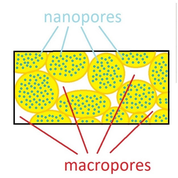

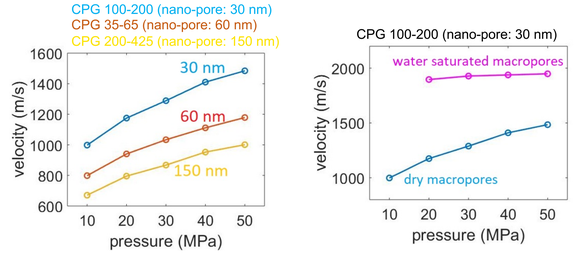

Water Content and Pressure

The ratios of the intensities of Q_3 and Q_4 signals are summarized in the table for both MAS and CP/MAS measurements. For all samples, except CPG 200- 425, after applying pressure, the Q_4 signal increases at the expense of the Q_3 signal. This indicates that silanol groups condense and release water.

While it is well-known that elevated temperatures lead to drying of silica by silanol condensation, it has not yet been described that applying pressure can have the same effect.

Sample	$Q_3 : Q_4$ (CP/MAS)	$Q_3 : Q_4$ (MAS)
CPG 35-60 Original	8.33	0.50
CPG 35-60 020419	4.00	0.38
CPG 100-200-Original-020719	5.56	0.53
CPG 100-200-020719	4.76	0.42
CPG 100-200-Water-020719	3.22	0.55
CPG 200-425 Original	2.94	0.36
CPG 200-425 020819	7.14	0.39

^{29}Si Solid-State NMR Spectroscopy

^{29}Si solid-state NMR spectroscopy is a powerful analytical method that allows the characterization of important solid materials, including minerals, silicones, and different types of silica. In this T3 project solid-state NMR has successfully been applied to study the impact of high pressures on silica materials.

The crucial signals of silica stem from **$[SiO]_2Si(OH)_2$** (Q_2), **$[SiO]_3Si(OH)$** (Q_3), and **$[SiO]_4Si$** (Q_4) groups.

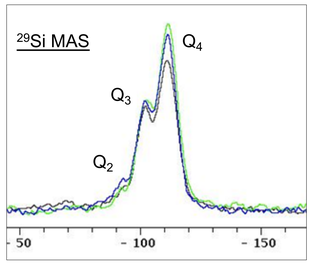

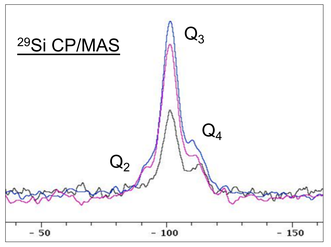

A representative ^{29}Si MAS (magic angle spinning) spectrum is shown above. The black line is the spectrum of the original sample CPG-100-200, the green trace results after applying pressure. The Q_4 grows as compared to the Q_3 signal. The blue spectrum stems from a hydrated sample.

In addition to MAS, the CP (cross polarization) technique can be applied that enhances the signal intensities of Q_2 and Q_3 by magnetization transfer from the Si-OH protons. The ^{29}Si CP/MAS spectra of the samples CPG-35-60 (pink line), CPG-100-200 (blue) and CPG-200-425 (black) are displayed above.

^{29}Si Lineshape Analysis and Deconvolution

In order to quantify the intensities of all overlapping signals in the ^{29}Si MAS and CP/MAS spectra, their lineshapes have to be analyzed by deconvolution.

An example for the signal deconvolution after simulation of the specific solid-state NMR lineshapes of the sample CPG 100-200-Water-020719 is shown here.

After deconvolution the relative signal intensities of Q_3 and Q_4 can be calculated (see Table on left).

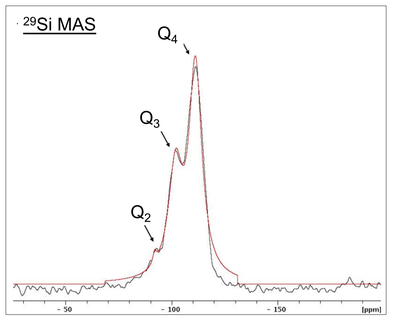

Multi-layer Deformation Tests

Triaxial compression tests are conducted on samples of multilayers of Indiana limestone and Carrara marble at confining pressure of 10 and 50 MPa (Jiao, unpublished data). At both pressure, multilayer-samples indicate strength between intact single layer of Carrara marble and Indiana limestone. At 10 MPa, multiple fractures are developed across the layers. At 50 MPa, strain partitioning occurs and more strain is accommodated in limestone layers.

Sample configuration
2 marble layers sandwiched between 3 limestone layers
Diameter: 18.8-18.9 mm
Total length: 35.64 mm
Layer thickness: 6.8-7.6 mm

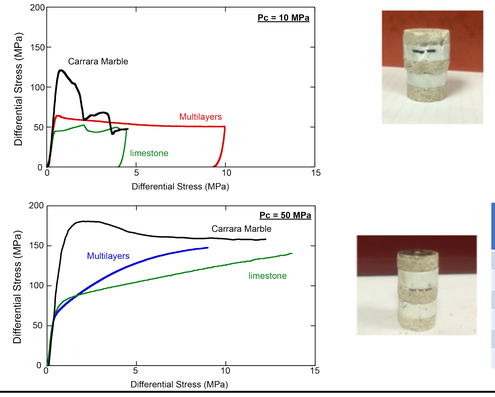

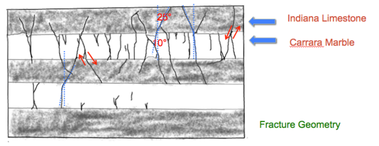

Layers	Initial thickness (mm)	Thickness after test (mm)	Axial strain (%)	Initial diameter (mm)	Diameter after test (mm)	Radial strain (%)
1 (Limestone)	7.62	6.93	9	18.82	19.43	3.2
2 (Marble)	7.62	7.49	1.7	18.92	19.53	3.2
3 (Limestone)	7.62	6.86	10	18.82	19.86	5.5
4 (Marble)	7.62	7.49	1.7	18.92	19.53	3.2
5 (Limestone)	7.62	6.86	10	18.82	19.69	4.6
Total	38.1	35.64	6.5			